View Article Online
View Journal

Dalton Transactions

An international journal of inorganic chemistry

Accepted Manuscript

This article can be cited before page numbers have been issued, to do this please use: F. G. Svensson, B. Greijer, T. Guerin, T. Agback, P. Agback and V. G. Kessler, *Dalton Trans.*, 2026, DOI: 10.1039/D6DT00402D.

ROYAL SOCIETY OF CHEMISTRY

rsc.li/dalton

View Article Online
DOI: 10.1039/D6DT00402D

Molecular mechanisms behind potential genotoxicity of metal oxide nanoparticles: nucleoside deglycosylation pathway

Fredric G. Svensson, Björn H. Greijer, Timothe Guerin, Tatiana Agback, Peter Agback, and Vadim G. Kessler*

Department of Molecular Sciences, Swedish University of Agricultural Sciences, Uppsala, Sweden

**Correspondence: vadim.kessler@slu.se*

Abstract – Polyoxometalates (POMs) represent well-defined molecular models for metal oxide nanoparticles and provide valuable insight into their interactions with biomolecules. Here, we investigate the interaction of Keggin-type phosphotungstic ($H_3PW_{12}O_{40}$) and silicotungstic ($H_4SiW_{12}O_{40}$) acids with RNA-derived nucleosides cytidine and guanosine, showing for the first time that these POMs can act as catalysts for the deglycosylation nucleosides and provide a possible molecular mechanism which facilitates this process. These systems provide useful molecular-level models for metal oxide nanoparticle–biomolecule interactions and potential RNA deglycosylation. Six crystalline complexes were obtained and structurally characterized by single-crystal X-ray diffraction, revealing extensive hydrogen bonding networks and pronounced interactions between nucleobases and the POM surfaces associated with charge transfer. In several cases, catalytic deglycosylation of nucleosides occurred during crystallization, yielding nucleobase–POM complexes and providing direct structural evidence of nucleoside cleavage. Complementary solution studies monitored by ^{1}H NMR demonstrated rapid and selective catalytic deglycosylation of guanosine by silicotungstate under acidic near-boiling conditions, following apparent first-order kinetics ($k = 0.399$ min^{-1}), whereas cytidine reacted rather slowly yielding only trace amounts of cytosine complexes. Phosphotungstate anion revealed analogous but slower reactivity. Control experiments showed no comparable catalytic activity for TiO_2 nanoparticle models (TiBALDH) under identical conditions. The results highlight pronounced differences in reactivity between purine and pyrimidine nucleosides and emphasize the role of charge-transfer and hydrogen-bonding interactions in POM-mediated catalysis. These findings provide molecular-level insight into metal oxide–biomolecule interactions and support the use of POMs as tunable models for understanding potential RNA degradation pathways induced by metal oxide nanoparticles.

Introduction

Small metal oxide nanoparticles have gathered much attention for their interactions with biomolecules, particularly in the context of therapeutic and diagnostic ("theranostic") applications.[1] Polyoxometalates (POMs), in particular, have been intensively studied for their antibacterial, antiviral, and anticancer properties where they can have complimentary or synergistic effects with conventional pharmaceuticals.[2-4]

View Article Online
DOI: 10.1039/D6DT00402D

The POMs are small, discrete oligonuclear metal-oxo species commonly with negative charge and a diameter from about 1 nm, making them suitable model systems for larger metal oxide nanoparticles. The chemistry of POMs is highly tailorable, making them very powerful tools for studying the interaction with biomolecules on the molecular scale. In some cases, the POM-biomolecule complex can be crystallized and thereby giving direct information about molecular interactions.[5-7] In particular, a variety of POMs have been studied for applications as nanozymes for peptide bond hydrolysis.[8, 9] Common minerals are also known to promote protein degradation.[10]

Recently, small anatase-TiO_2 nanoparticles were demonstrated to possess significant antiviral activity towards the enveloped transmissible gastroenteritis virus but not to the non-enveloped encelomyocarditis virus. Complexation between envelope phospholipids and TiO_2, with the subsequent disruption of the viral envelope, was proposed as the mechanism for this inhibitory effect.[11] POMs are well-known for several decades to inhibit a range of different RNA-viruses.[12]

There is an ongoing discussion concerning cytotoxicity of TiO_2 NPs and their potential to cause DNA strand breakage.[13] TiO_2 has generally been considered safe for cosmetic and food applications, e.g. UV-adsorber in sunscreens and food additive. However, its safety has recently been questioned with claims of various negative consequences upon extended or high-dose exposure.[14] Interaction with cell membrane and receptors, as well as cytotoxicity via formation of oxygen radicals via photoactivation appears to be the main hazards.[15] Lojk et al.[16] studied the uptake and effects of several nanoparticles (SiO_2, Ag, and TiO_2) on human neural cells. They concluded that even at low exposure (2−10 μg/ml), but especially under prolonged exposure, these nanoparticles could negatively affect the cells. Some recent works have reported DNA damage caused by TiO_2 nanoparticles.[17-19] However, a study by Rajapakse and co-workers[20] concluded that erroneously conducted single cell gel electrophoresis assay ("Comet assay") used to detect DNA damage can cause false positives, especially if not complemented with other biomarkers for DNA damage. Naya and co-workers[21] investigated the effect of intratracheal instillation of anatase TiO_2 in rats. While the exposure induced inflammation, no DNA damage was found. However, UV-illumination of TiO_2 is known to cause DNA damage and strand breaks by generation of reactive oxygen species.[22, 23]

In the present study, we have investigated the interaction between a pyrimidine (cytidine) and a purine (guanosine) derived RNA nucleosides, with the Keggin POMs represented by phosphotungstic acid and silicotungstic acid. The purpose was to use these as model system for the potential catalysis of deglycosylation reaction (RNA breakage) catalyzed by metal oxide nanoparticles. The deglycosylation reaction (the removal of a sugar group from, usually a biomolecule) occurs naturally for purines and pyrimidines, although at very slow rates, but can be greatly accelerated by enzymes or catalysts.[24, 25] UV-illumination and hydrolytic oxidation can also cause deglycosylation with potential resulting RNA/DNA.[26, 27] Deglycosylation is performed enzymatically by DNA glycosylases as part of the base excision repair mechanism to remove damaged nucleobases.[28] For RNA, the N-glycosidic bond can be cleaved by RNA *N*-glycosidases.[29]

View Article Online
DOI: 10.1039/D6DT00402D

The spherical metal oxo-anions of about 1 nm provide excellent models for metal oxide nanoparticles for studying interaction between biologically relevant molecules. Phosphotungstic acid and silicotungstic acid bearing different charge (–3 and –4 respectively) and displaying different polarity of metal-oxygen bond were specifically chosen in the view also of their earlier proved ease of crystallization with various biomolecules. As a comparison, titanium(IV) "bis(ammonium lactate)dihydroxide" (TiBALDH) was used specifically as model for TiO_2 nanoparticles, as TiBALDH exists in a coordination equilibrium with TiO_2 nanoparticles of about 3 nm in size.[30] In this work, we aimed at isolating POM-nucleobase complexes and evaluating the potential stability and transformation pathways. We present the first observation of the catalytic function of two POMs, silicotungstic acid and phosphotungstic acid, for the deglycosylation reaction of nucleobases (cytidine and guanosine) and propose a possible molecular interaction pathway that facilitates the process.

Materials and Methods

Chemicals

Phosphotungstic acid (ThermoScientific, p.a., CAS: 12501-23-4), silicotungstic acid (Sigma-Aldrich, p.a., CAS: 12027-43-9), hydrochloric acid (Supelco, 37 %, CAS: 7647-01-0), cytidine (Sigma-Aldrich, 99%, CAS: 65-46-3), guanosine (Sigma-Aldrich, 98%, CAS: 118-00-3), dopamine hydrochloride (Aldrich, 98 %, CAS: 62-31-7), TiBALDH (Sigma-Aldrich, 50 wt%, CAS: 65104-06-5). The general synthetic procedure is illustrated in Scheme 1.

Preparation of molecular models

Compound **1,** [(HCytidine)$_3$PW$_{12}$O$_{40}$]: 0.109 gram (0.59 mmol) cytidine and 0.432 gram (0.150 mmol, 3 mM) phosphotungstic acid were mixed in 50 mL 0.1 M HCl. The mixture precipitated (yellow), and was heated to 95^{o}C to dissolve, then allowed to cool to room temperature slowly in a Dewar. The pH of the freshly prepared solution was 1.40.

Compound **2**, [(HCytidine)HPW$_{12}$O$_{40}$•H$_3$O]: 0.144 gram (50 µmol, 1.1 mM) phosphotungstic acid was dissolved in 10 mL 0.1 M HCl, and 0.012 gram (50 µmol) cytidine in 35 mL 0.1 M HCl. Added the phosphotungstate solution to the cytidine solution. No precipitation occurred and the pH of the colorless freshly prepared solution was 1.41. The solution was allowed to evaporate over several weeks until crystals formed.

Compound **3**, [(HCytosine) PW$_{12}$O$_{40}$•2H$_3$O]: Identified as a fraction in 2 after several attempts of re-crystallization by dissolving in 0.1 M HCl on heating and subsequent slow cooling.

Compound **4**, [(HGuanine)H$_2$PW$_{12}$O$_{40}$]: 0.288 gram phosphotungstic acid (100 µmol) with 0.08 gram (28.2 µmol, 2 mM) guanosine and were dissolved in 50 mL 0.1 M HCl. The pH of the freshly prepared solution was 1.36. Yellow precipitate formed, which was dissolved by heating to 95^{o}C. The solution turned orange as it cooled, and orange crystals formed at 85^{o}C. The

View Article Online
DOI: 10.1039/D6DT00402D

solution was cooled to 70°C over several hours, then allowed to cool to room temperature. This treatment appears to have removed the sugar group from guanosine, and only the guanine base is visible in the structure.

Compound **5,** $[(Cytidine)_6(Dopamine)(SiW_{12}O_{40})_2 \bullet 9H_2O]$: 100 mg of silicotungstic acid (34 µmol, 6.9 mM) was mixed with 1 eq. cytidine (8 mg, 34 µmol) and 0.5 eq (7 mg, 17 µmol) dopamine in 5 mL 0.1 M HCl. This colorless solution with a pH of 1.36 was left on a Petri dish for slow evaporation. Small, colorless needles were formed after about 2 weeks.

Compound **6**, $[(Guanine)_2(SiW_{12}O_{40})_2 \bullet 16H_2O]$: 100 mg of silicotungstic acid (34 µmol, 6.9 mM) in 5 mL 0.1 M HCl was mixed with 1 eq. of guanosine (10 mg, 34 µmol). A yellow precipitate formed and the initial pH was 1.38. This solution was transferred into a glass tube and kept in a water bath at ca. 100°C for 15 minutes, then cooled down to room temperature. After several months, small, pale yellow needle crystals formed.

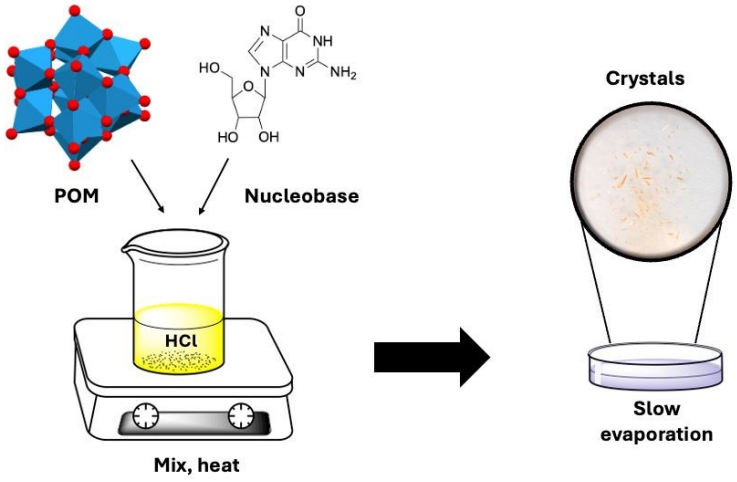

Scheme 1. General procedure for preparation of compound **1** to **6**.

X-ray single crystal studies

All experiments were carried out at room temperature with Bruker D8 Quest ECO diffractometer operating with MoKα-radiation (λ = 0.71073 Å). The details of data collection and refinement are summarized in Table 1 and in the Supplementary Information. The initial solutions for all structures were obtained using direct methods, producing tungsten and heavy heteroelements, P or Si respectively, positions. All other non-hydrogen atom positions were identified in subsequent difference Fourier syntheses. The hydrogen atoms on the organic molecules were added through geometrical calculations where possible. No hydrogen atoms could be located on interstitial water molecules. The structure of Compound **1**, featuring 3 protonated cytosine cations per phosphotungstate anion showed no disorder. The B-alerts in CheckCif are caused solely by the impossibility to locate active hydrogen atoms on the sugar unit and interstitial oxygen atoms. Crystals of compound **2** were notoriously difficult to investigate due, on one hand, to rapid decomposition under X-ray beam at room temperature and

View Article Online
DOI: 10.1039/D6DT00402D

cracking on cooling preventing possibility to use cryo-system to obtain more complete data. This resulted in limited completeness of the data. This structure is an example of hydrogen-bonded metal-organic framework with tunnel shaped pores ca. 12 Å in diameter. The residual electron density in pores is quite low, indicating that they are essentially empty in air-dried crystals. The crystals of compound **3** were discovered as minor impurity in the samples of **2** subjected to repeated re-crystallization by re-dissolution on reflux in water with subsequent slow cooling. This structure is free from disorder and does not contain additional oxygen atoms. There is only one symmetrically independent cytidine cation in a general position without disorder. The CheckCif does not contain any A or B alerts. Compound **4** is chemically an analog of **3** with guanine instead of cytidine molecules. The structure is, however, heavily disordered with one guanine molecule in general position distributed equally between 3 partially overlapping locations. The other two are in special position around a center of symmetry, overlapping with themselves, which excluded possibility to locate hydrogen atoms and causing the reported B-alerts in CheckCif. Compound **5** is a rare case of highly asymmetric polar structure with P1 as space group. Crystallization of silicotungstate complexes can be rather difficult, in the view of high charge of the anion easily resulting in formation of a glassy solid. Therefore, a small amount of more symmetric dopamine molecules has been added to change the sterical conditions of packing. The resulting product contains 5 cytosine and one dopamine cations along with 4 phosphotungstate anions, resulting in 1.25 ligand-to-POM (or cation-to-anion) ratios, close to those in the structure of **2**. The structure of compound **5** is thus close to trigonal but severely distorted resulting in P1 symmetry. Compound **6** is a clathrate structure with extremely high water content. Data collection was only possible on a crystal sealed in into a capillary with a droplet of mother liquor on the bottom. Powder diffraction patterns were collected for compounds **2**, **4**, and **6** by placing crystals in glass capillaries. Theoretical powder diffractograms were calculated in CCDC Mercury version 2025-2.0.

Representative nature of the performed X-ray single crystal studies for the whole samples of produced crystals was additionally confirmed by recording at least 5 short diffraction experiments for each of the materials randomly selecting crystals from the samples. Unit cell parameters were in each case coinciding within the standard deviations.

Full details of data collection and treatment in X-ray studies reported in this manuscript are available free-of-charge from the Cambridge Crystallographic Data Centre at https://www.ccdc.cam.ac.uk citing deposition numbers: **2530303-2530308**.

Deglycosylation experiments

For the deglycosylation experiments, 100 mg (ca. 7 mmol) of phosphotungstate, silicotungstate, or the equivalent amount of titanium(IV) “bis(ammonium lactate)dihydroxide” (TiBALDH) was added to 5 mL of 0.1 M HCl with 1 equivalent of cytidine or guanosine in a glass test tube. The tubes were placed in a stirred water bath holding approximately 100^{o}C. Cytidine dissolved readily in 0.1 M HCl, but guanosine required heating to about 60^{o}C before

View Article Online
DOI: 10.1039/D6DT00402D

dissolving. For the kinetic experiment, aliquots 0.5 mL solution was extracted at 1, 3, 5, 8, 12, and 20 minutes to Eppendorf tubes which were snap-frozen in liquid nitrogen and stored in a freezer (–18°C) until NMR analysis.

NMR analyses

The reaction solutions were analyzed with ^{1}H NMR, employing a Bruker Avance III 600 MHz spectrometer with Bruker TopSpin version 3.5. For sample preparation, 450 µL sample solution was mixed with 50 µL D_2O (Eurisotope) in a 3 mm NMR tube. For the reaction kinetics experiment, DMSO was used as internal standard for the kinetics experiment. The spectra were processed and analyzed in the Bruker TopSpin version 4.0 software.

FTIR analysis

Transmission FTIR analyses of crystals and precipitates were done by griding crystals or precipitate in dried KBr (200°C, overnight) and pressing them to pellets (10 ton applied pressure for 3 minutes). A Perkin–Elmer FTIR spectrometer Spectrum-100 was used to record the IR spectrum. Pure KBr was used for background subtraction. The spectra were recorded from 400 cm^{-1} to 4000 cm^{-1} with 1 cm^{-1} resolution and 16 scans per spectrum.

Results and Discussion

Structural comments

Compound **1,** $[(HCytidine)_3PW_{12}O_{40}]$, (Figure 1) crystallized in the orthorhombic space group P212121 as yellow plates. It contains 3 cytidine molecules per POM. The amino groups are protonated to balance the –3 charge of the POM. However, the structure contains no solvent water molecules. The structure features an extended network of hydrogen bonds between the POM and cytidine, where the nucleobase ammonium group and the ribose hydroxyl groups. Hydrogen bonding also occurs between cytidine molecules via ribose hydroxyls and nucleobase imine function. The shortest distances between the POM and nucleoside were in the following bond; N3C-O31 3.277 Å (terminal O), (C5C)H5CB-O32 2.238 Å (bridging O) the direct C209-O32 contact being 3.100Å, (O2C)H2CB-O19 2.736 Å, (terminal O) (Supplementary Figure S1).

View Article Online
DOI: 10.1039/D6DT00402D

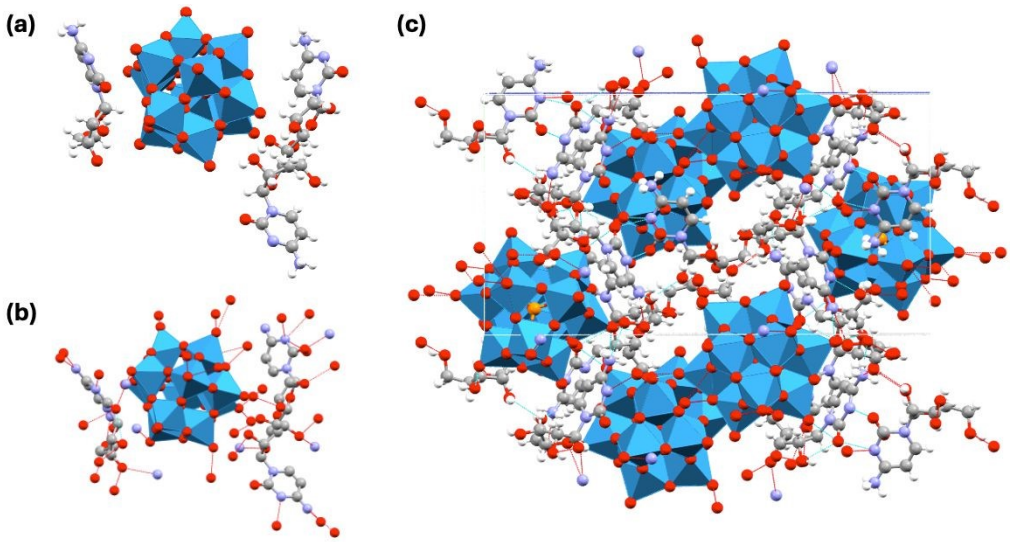

Figure 1. Molecular structure of **1** [(HCytidine)$_3$PW$_{12}$O$_{40}$] (a), hydrogen bonding in **1** (b), and packing with hydrogen bonding in **1** (c). Turquoise is W, red is O, orange is P, grey is C, blue is N, and white is H.

Compound **2**, [(HCytidine)HPW$_{12}$O$_{40}$•H$_3$O], (Figure 2) crystallized in trigonal space group P3 as yellow needles. Like in structure **1**, cytidine has one protonated amino group, which with one oxonium ion balances the 2 negative charges of the POM. The packing features a hydrogen bonded framework between cytidine, POM and solvent water. The cytidine ammonium groups hydrogen bond to bridging oxygen atoms in the POM. The solvating oxonium ion hydrogen bonds to the nucleobase imine group. The amino bases are tilted in a face-on mode towards the POM, revealing substantial π-metal interactions. The aromatic ring acts as an π-acceptor of negative charge from polarized W-O bonds on the POM. From the extended packing in Figure 2c is can be seen that compound 2 forms an open MOF-like structure. The shortest distances between the POM and nucleoside were in the following bond; N202-O35 3.435 Å (terminal O), N202-O48 3.469 Å (bridging O), (C209)H209-O21 2.869 Å (bridging O) (C208)H208-O21 3.385 Å (bridging O) (Supplementary Figure S2).

View Article Online
DOI: 10.1039/D6DT00402D

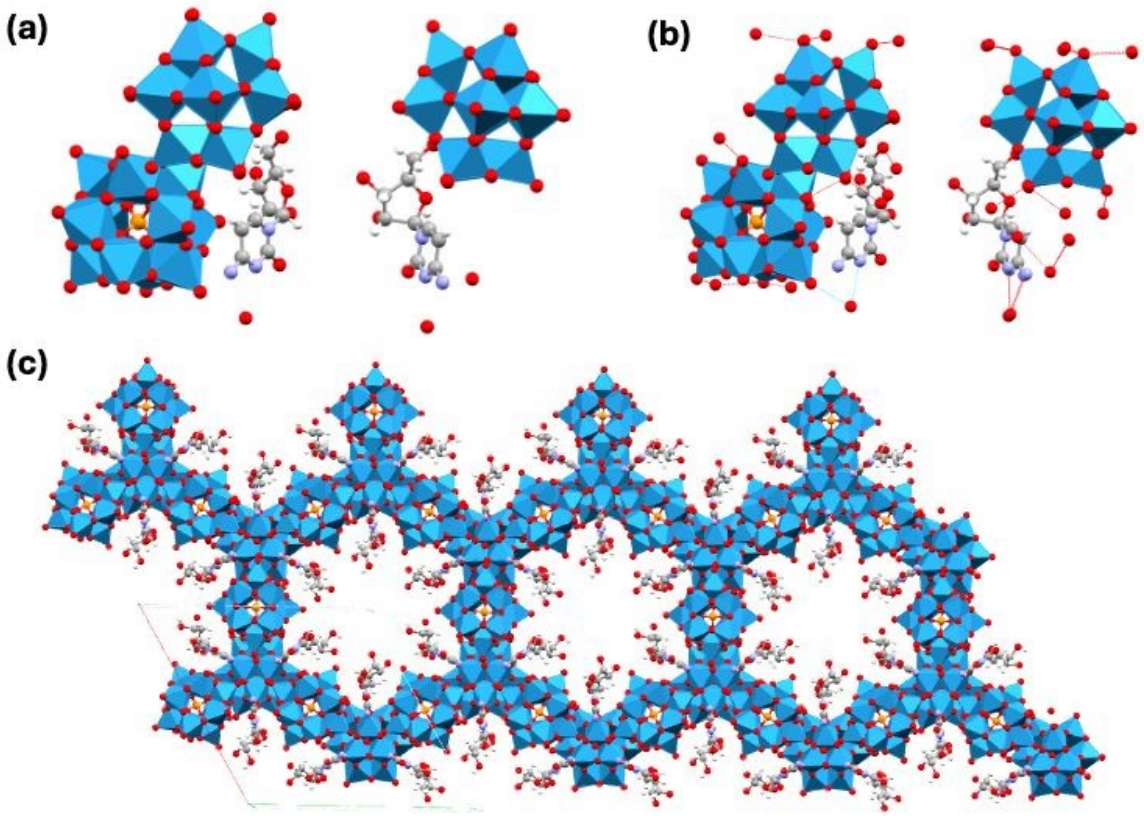

Figure 2. (a) Molecular structure of **2**, [(HCytidine)$HPW_{12}O_{40}$•H_3O] (b) hydrogen bonding in **2**, and (c) extended packing of **2** along the b-direction. Turquoise is W, red is O, orange is P, grey is C, blue is N, and white is H.

Compound **3**, [(HCytosine)$H_2PW_{12}O_{40}$], (Figure 3) crystallized in trigonal space group R-3 as yellow block crystals in trace amounts along with **2** after prolonged reflux in acidic medium. In this structure, the cytidine has been cleaved into cytosine, which crystallized in a 1:1 ratio with phosphotungstate. The ribose part was not present in the structure. The packing is rather compact with altering layers of phosphotungstate and cytosine. Also, for compound **3**, the cytosine aromatic ring is turned towards the POM, again forming charge-transfer complex. Additionally, the amino group hydrogen bonds to both bridging and terminal oxygens on the POM. Hydrogen bonding also occurs between cytosine molecules, from the amino group to the carbonyl oxygen. The shortest distances between the POM and nucleoside were in the following bond; (N1)H1B-O14 2.783 Å (bridging O), (N3)H3A-O1 2.645 Å (terminal O), N2-O9 3.454 Å (bridging O) (Supplementary Figure S3).

View Article Online
DOI: 10.1039/D6DT00402D

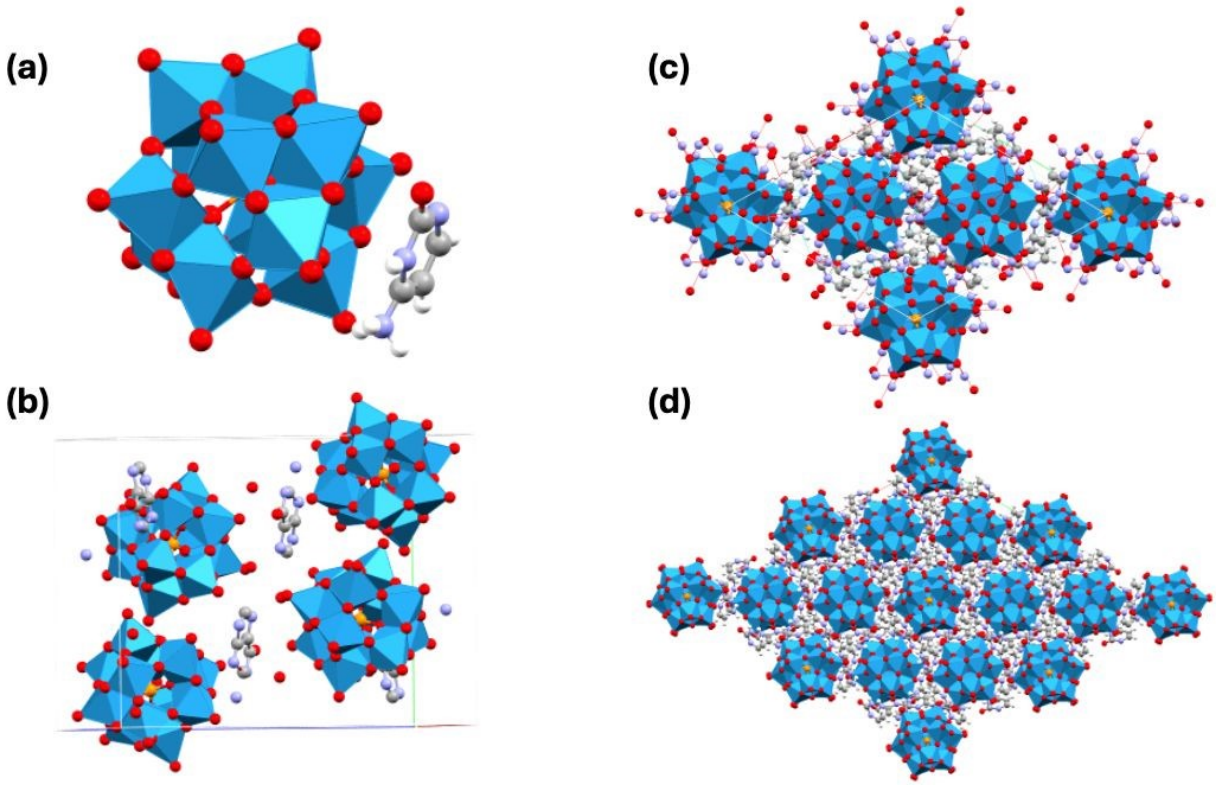

Figure 3. (a) Molecular structure of **3**, [(HCytosine)$H_2PW_{12}O_{40}$], (b) packing of **2**, (c) packing of **2** with hydrogen bonds, and (d) extended packing of **3**. Turquoise is W, red is O, orange is P, grey is C, blue is N, and white is H.

Compound **4**, [(HGuanine)$PW_{12}O_{40}$•$2H_3O$], crystallized in the monoclinic space group P21/n as orange needles (Figure 4). The guanine molecule is heavily disordered over several positions. The –3 negative charge on the phosphotungstate is balanced by a protonated amine group on guanine and two oxonium ions. The guanine molecules are located face-on towards the POM, which together with the orange color reveal charge-transfer interaction. However, the guanine amino group hydrogen bonds to bridging oxygens on the POM. The solvating oxonium ions hydrogen bonds to the POM, but not the guanine. The extended structure forms alternating layers of POMs and guanine. The shortest distances between the POM and nucleoside were in the following bond; N1A-O016 3.555 Å (terminal O), N2A-O00V 3.718 Å (bridging O), N3A-O01F 3.399 Å (Supplementary Figure S4).

View Article Online
DOI: 10.1039/D6DT00402D

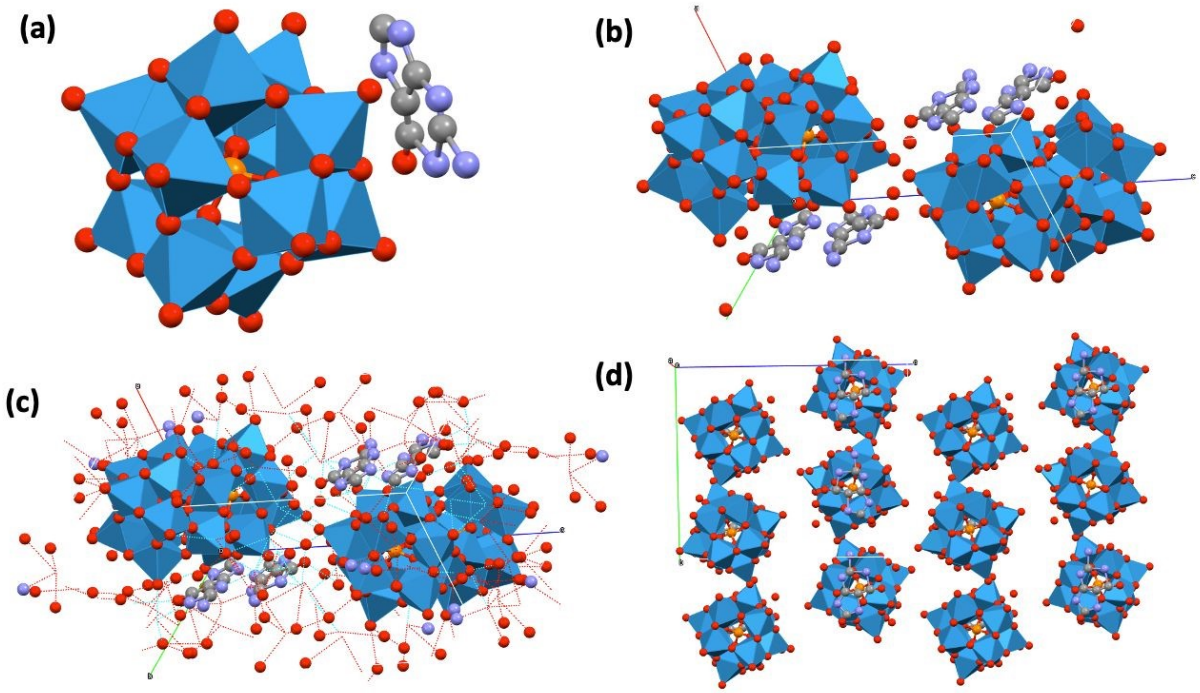

Figure 4. (a) Molecular structure of **4**, [(HGuanine)$PW_{12}O_{40}$•$2H_3O$], (b) packing of **4**, (c) hydrogen bonding in **4**, and (d) extended packing of **4** in the c-direction. Turquoise is W, red is O, orange is P, grey is C, and blue is N. The heavy disorder in the guanosine molecule has been omitted for clarity.

Compound **5,** [$(HCytidine)_6(HDopamine)(SiW_{12}O_{40})_2$•$9H_2O$], (Figure 5) crystallized in the triclinic space group P1 as colorless needles. Dopamine was added as 0.5 equivalents to phosphotungstate and cytidine in an attempt to stabilize the 1:1 complex between phosphotungstate and cytidine. We previously utilized this strategy to prepare the 1:1 gamma-aminobutyric acid: phosphotungstate complex which was unobtainable without the addition of dopamine (despite dopamine itself did not made part of the crystal).[31] The cytidine nucleobases are turned face-on towards the POM, indicating π-metal interactions. However, as the crystals are colorless, so the electronic transition appears to lie outside the visible region. Hydrogen bonding occurs between cytosine amino groups and bridging POM oxygen atoms. Hydrogen bonding also occurs between cytosine molecules via the amino groups and carbonyl oxygens. The shortest distances between the POM and nucleoside were in the following bond; (CF5)H5FA-O15A 2.904 Å (terminal O), N1F-O21A 3.351 Å (bridging O), (C4F)H4F4-O21A 3.302 Å (bridging O) (C4F)H4F4-O36A 3.338 Å (terminal O), N3F-H3F3-O22A 2.715 Å (terminal O) (Supplementary Figure S5).

View Article Online
DOI: 10.1039/D6DT00402D

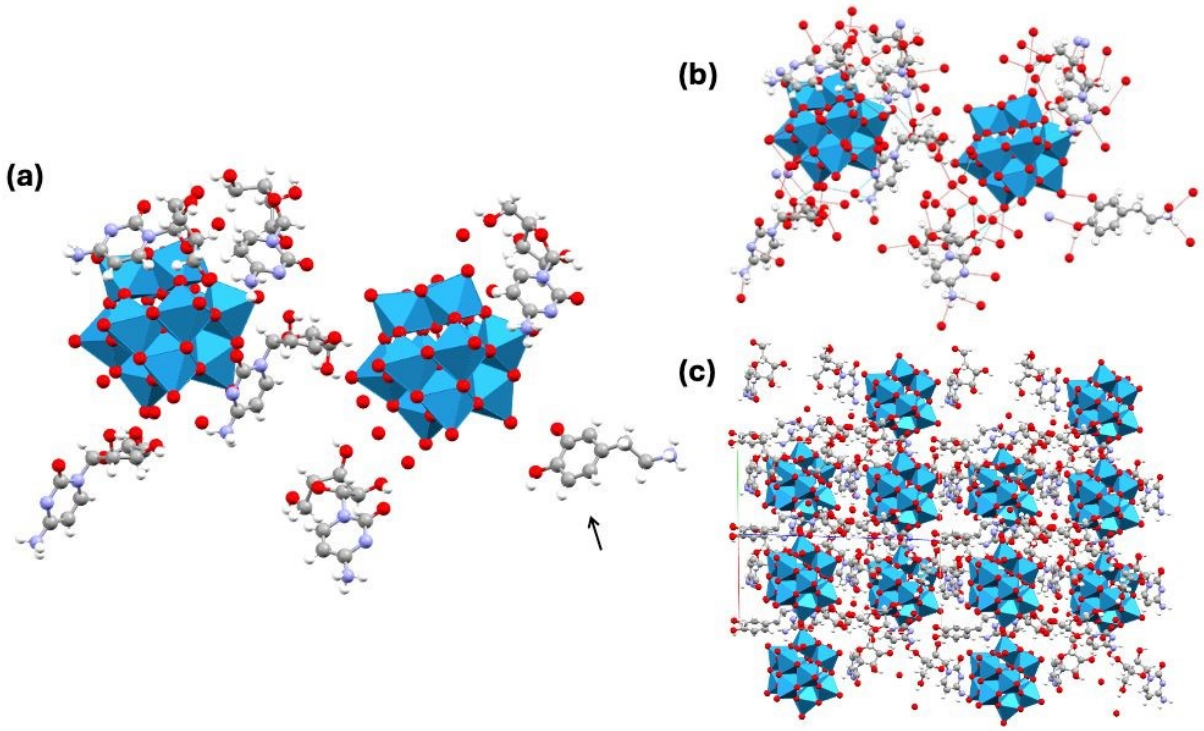

Figure 5. (a) Structure molecular of **5,** $[(HCytidine)_6(HDopamine)(SiW_{12}O_{40})_2 \bullet 8H_2O(H_3O)]$, (b) packing of **5**, and (c) packing of **5** with hydrogen bonding. Turquoise is W, red is O, gold is Si, grey is C, blue is N, and white is H. The arrow indicates the lone dopamine group.

Compound **6**, $[(HGuanine)_2(SiW_{12}O_{40}) \bullet 14H_2O(H_3O)_2]$ (Figure 6) crystallized in the monoclinic space group P 21/n as small, pale-yellow needles. The unit cell contains 16 water molecules, and the crystals quickly degrade by water loss at ambient conditions. The experiment was carried out by sealing a crystal in an X-ray transparent borosilicate capillary, where a drop of mother liquor was placed in the bottom. Silicotungstate crystallized after several months with guanine formed through the catalytic deglycosylation of guanosine at high temperature. Like in the previous structures, the nucleobase is turned face-on towards the POM. The yellow color indicates some charge-transfer. There is extensive hydrogen bonding in compound **6**. Guanine bonds via its amino group to bridging oxygens in the POM, to carbonyl group of neighboring guanosines and to solvent water/oxonium ions via both the ammonium and carbonyl groups. The shortest distances between the POM and nucleoside were in the following bond; N12-O38 3.169 Å (terminal O), N12-O22 3.252 Å (bridge O), N13-O2 3.192 Å (terminal O), (N14)H14A-O2 2.760 Å (terminal O), (N11)H11C-O22 3.127 Å (bridge O) (Supplementary Figure S6).

A general comment that should be given concerning the short contacts is that they mostly are due to hydrogen bonds between more acidic H-atoms at the protonated nucleobases and, in the first hand, bridging, more negatively charged oxygen atoms of POMs. An important additional phenomenon most apparent in the structure of compound **1** is a rather short distance between a

View Article Online
DOI: 10.1039/D6DT00402D

bridging oxygen atom O32 in the structure of POM and the carbon atom by which the sugar is connected to the nucleobase, C5C. This interaction points at the effect of POM as nucleophile in catalysis of the splitting of this C-N bond.

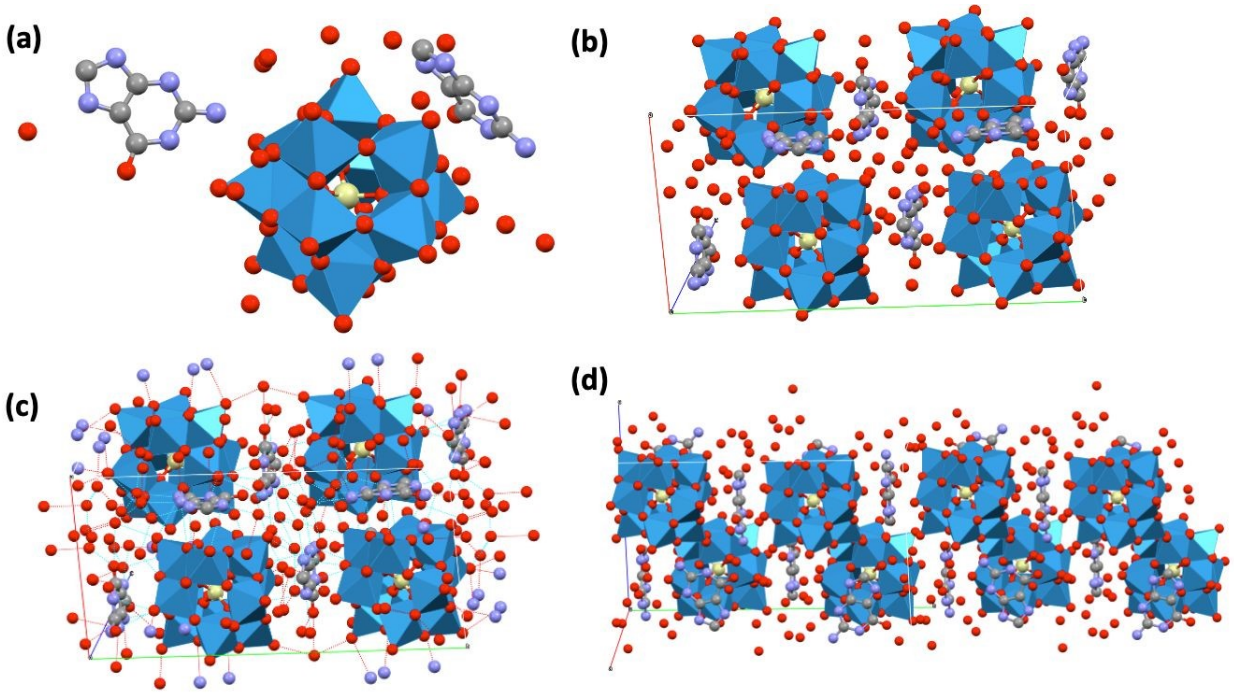

Figure 6. (a) Structure molecular of **6,** [(HGuanine)$_2$($SiW_{12}O_{40}$)•$14H_2O(H_3O)_2$], (b) packing of **6**, (c) packing of **6** with hydrogen bonding, and (d) extended packing in the b-direction. Turquoise is W, red is O, gold is Si, grey is C, blue is N, and white is H.

Table 1. Crystallographic data of **1-6**. Additional crystallographic data is available in the Supplementary Information Table S1 through S28.

Compound	1	2	3	4	5	6
Composition	$C_{27}H_{42}N_9O_{55}PW_{12}$	$C_9H_{14}N_3O_{41.33}P_{0.83}W_{10}$	$C_{12}H_{18}N_9O_{43}PW_{12}$	$C_{15}H_{22}N_{15}O_5P_{12}$	$C_{53}H_{94}N_{16}O_{121}Si_2W_{24}$	$C_{10}H_{45}N_{10}O_{58}SiW_{12}$
Formula weight	3609.86	2689.87	3213.52	3369.65	7360.2	3467.85
Crystal system	Orthorhombic	Trigonal	Trigonal	Monoclinic	Triclinic	Monoclinic
Space group	$P2_12_12_1$	P3	R-3	$P2_1/n$	P1	P21/n
R1	0.0379	0.0499	0.0239	0.0781	0.087	0.0396
wR2	0.0901	0.1362	0.0643	0.2269	0.1061	0.1105
GooF	1.148	1.034	1.054	1.035	1.009	1.107
a (Å)	13.5434(9)	25.309(3)	19.0192(9)	12.658(4)	13.097(5)	12.9065(17)
b (Å)	15.7745(11)	25.309(3)	19.0192(9)	18.893(6)	13.156(5)	24.994(3)
c (Å)	29.268(2)	15.307(2)	0.9800(14)	23.363(7)	23.538(9)	17.585(2)
α (◦)	90	90	90	90	94.428(15)	90
β (◦)	90	90	90	105.494(6)	90.250(15)	95.890(6)
γ (◦)	90	120	120	90	112.309(14)	90
V (Å)	6252.9(7)	8491(2)	6572.3(2)	5384(3)	3738(3)	5642.8(13)
T (K)	295(2)	296(2)	295(2)	295(2)	293(2)	295(2)
Z	4	6	6	4	1	4
Nr. refl.	9952	9561	9343	9247	8512	9329
θ min	2.42	2.28	2.66	2.34	2.46	2.47
θ max	32.82	25.38	39.44	26.73	33.40	37.73
CCDC reference	**2530303**	**2530304**	**2530306**	**2530305**	**2530307**	**2530308**

View Article Online
DOI: 10.1039/D6DT00402D

Table 2. Selected short distances between POM oxygens and nucleobases. These are shown in Supplementary Figures S1 thought S6.

Compound 1	Compound 2	Compound 3	Compound 5	Compound 4	Compound 6
N3C–O31 3.277 Å	N202–O35 3.435 Å	(N1)H1B–O14 2.783 Å	(CF5)H5FA–O15A 2.904 Å	N1A–O016 3.555 Å	N12–O38 3.169 Å
(C5C)H5CB–O32 2.238 Å	N202–O48 3.469 Å	(N3)H3A–O1 2.645 Å	N1F–O21A 3.351 Å	N2A–O00V 3.718 Å	N12–O22 3.252 Å
(O2C)H2CB–O19 2.736 Å	(C209)H209–O21 2.869 Å	N2–O9 3.454 Å	(C4F)H4F4–O21A 3.302 Å	N3A–O01F 3.399 Å	N13–O2 3.192 Å
	(C208)H208–O21 3.385 Å		(C4F)H4F4–O36A 3.338 Å		(N14)H14A–O2 2.760
			(N3F)H3F3–O22A 2.715 Å		(N11)H11C–O22 3.127

FTIR analyses of complexes

Compounds **2, 3**, **5** and **6** were obtained in large enough amounts for FTIR analysis (Figure 7). A strong, quite broad band at ca. 800 cm^{-1} is assigned to W-O-W bending of the phosphotungstate ion. At 920 cm^{-1}, a sharp, strong signal is seen for terminal W=O. Another sharp band located at 1089 cm^{-1} is assigned to the P–O stretch, this is obviously absent in compound **5**, where the central phosphorous ion is replaced by Si. At about 1605 cm^{-1}, a small band from the C=C stretching of the aromatic rings is seen as well as a small band from the organic carbonyl groups at ca. 1720 cm^{-1}. A weak band for the C–N stretch is seen at 1270 cm^{-1}, originating from the purine and pyrimidine rings of the nucleobase, and the amine group in dopamine. As the samples were dried prior to analysis, the water content is rather low.

View Article Online
DOI: 10.1039/D6DT00402D

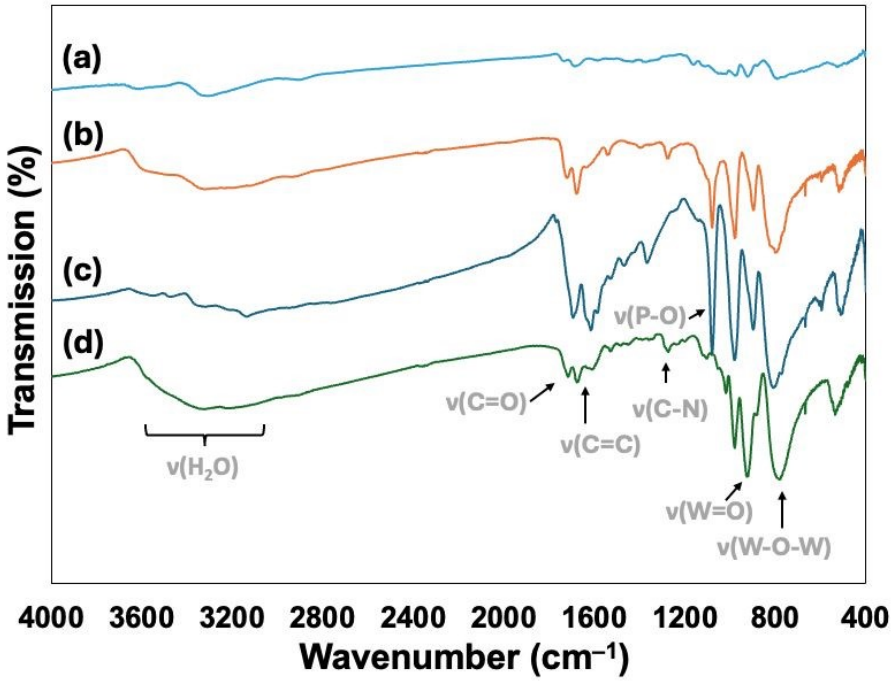

Figure 7. FTIR spectra of (a) compound **6**, (b) compound **2**, (c) compound **3,** and (d) compound **5**. Major adsorption bands are indicated.

Catalytic studies

The potential catalytic deglycosylation of guanosine and cytidine with two different POMs (silicotungstate and phosphotungstate) or TiBALDH was investigated (Figure 8). The reaction was monitored by ^{1}H NMR by observing the decrease in the intensity of the proton resonance at ca. 6.1 ppm corresponding to H1', which is covalently bonded to the C1' carbon of the ribose ring (Scheme 2). Upon deglycosylation, this carbon replaces the nucleobase with and –OH group. Initially, the reaction was tested at 37^{o}C as this is relevant for biological systems. However, no reaction was observed at this temperature. When the reaction temperature increased to ca. 100^{o}C, guanosine was observed to undergo deglycosylation in the presence of silicotungstate (Figure 8). Cytidine, on the other hand, remained intact even at this temperature. However, as revealed by the crystal structure of compound **3**, cytidine will during long storage together with phosphotungstate in acidic medium undergo deglycosylation, although at a much slower rate than guanosine.

No change has been observed in the ^{1}H NMR spectrum of guanosine at 0.1 M HCl at 100^{o}C without silicotungstate, indicating it acts as a catalyst. Since silicotungstic acid is a strong acid, and potentially could increase the acidity, pH was measured for guanosine in 0.1 M HCl and guanosine with SiW in 0.1 M HCl. In all cases, pH was 1.4 ± 0.2, suggesting the reaction was not caused by a decreased pH, but rather a catalytic function induced by silicotungstate.

Guanosine is poorly soluble in water and requires dilute HCl as solvent. Clear solutions were obtained first above 60^{o}C. Mixing 1 eq. of guanosine with TiBALDH diluted in deionized water caused a cloudy suspension which cleared up upon heating. At 100^{o}C the solution was clear but

View Article Online
DOI: 10.1039/D6DT00402D

as it was cooled down to room temperature, a white fluffy precipitate formed. This precipitate was washed (with deionized water), dried at 60°C and analyzed by transmission FTIR (Figure 9). Comparing the precipitate with reference guanosine revealed the precipitate to be pure guanosine. The ^{1}H NMR spectra from the supernatant found only trace amounts of guanosine. Thus, under the present conditions, TiBALDH could not promote deglycosylation of neither guanosine nor cytidine. The oxygen atoms in the titania Ti-O bonds are expected to be more negative than the (Si)W-O oxygens. However, anatase TiO_2 has an isoelectric point of 5.9 to 6.2[32] and the surface oxygens would therefore be protonated at acidic conditions. A catalytic activity at higher pH cannot be ruled out.

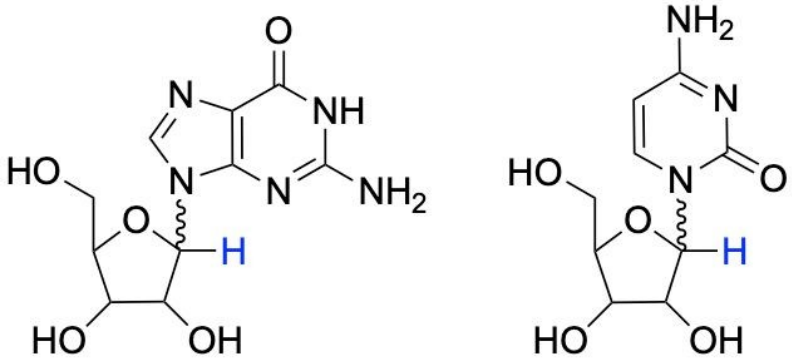

Scheme 2. Structures of (a) guanosine and (b) cytidine. The 1' proton is highlighted in blue.

View Article Online
DOI: 10.1039/D6DT00402D

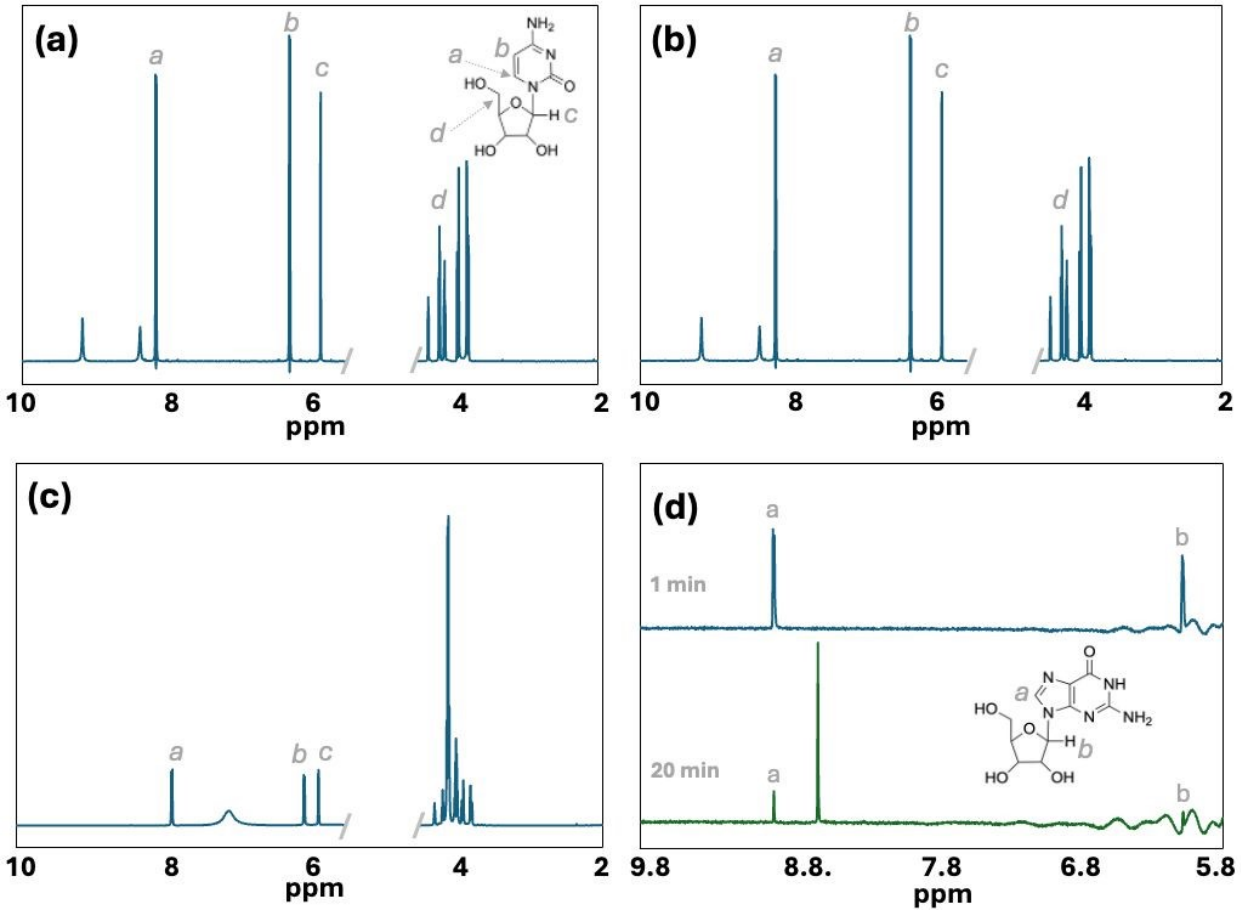

Figure 8. ^{1}H NMR of (a) phosphotungstic acid with cytidine (1:1 at 100°C), (b) silicotungstic acid with cytosine (1:1 at 100°C), (c) TiBALDH with cytidine (1:1 at 100°C), and (d) silicotungstic acid with guanosine (1:1) after 1 and 20 min at 100°C. The water region from 4.5 ppm to 5.5 ppm was cut out in (a), (b), and (c) for clarity.

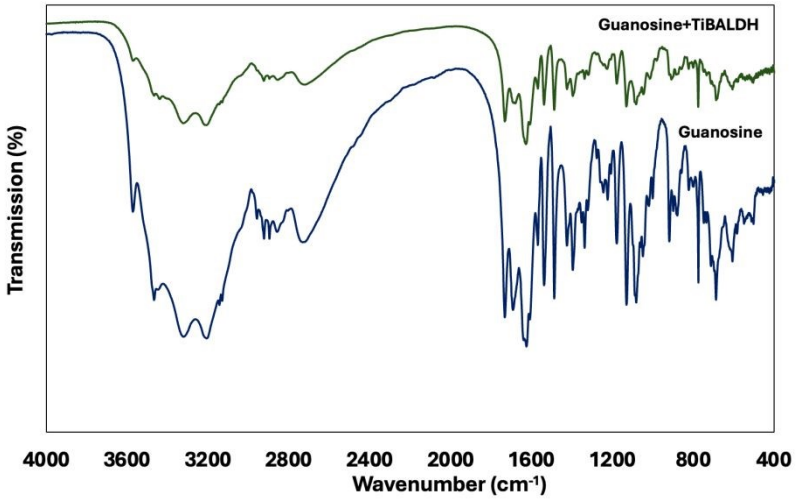

Figure 9. Comparison of the FTIR spectra between reference guanosine and the precipitate after boiling guanosine with TiBALDH in basic medium.

View Article Online
DOI: 10.1039/D6DT00402D

While cytidine remained stable, guanosine decomposed in the presence of silicotungstate under near-boiling conditions. To obtain a better understanding of the reaction, kinetic experiments were carried out. Small volumes were extracted from the reaction at different time points for 20 minutes. Since guanosine did not dissolve instantaneously, the first time point was set to 1 minute after adding it to the pre-heated silicotungstate solution. The kinetics were based on the decreasing 1' hydrogen signal from the ^{1}H NMR spectra, using DMSO as internal standard. As seen in Figure 10a, the reaction is fast and is almost completed within 5 minutes. It approximately follows the first-order reaction kinetics (Figure 10b). The rate constant was determined to 0.399 min^{-1} from the slope of the first-order plot. The deglycosylation reaction of guanosine with silicotungstic acid is shown in Scheme 3. Kinetics was performed on the mixture of phosphotungstic acid with guanosine using the same experimental conditions as for silicotungstic acid and guanosine. It was, however, complicated due to the formation of massive precipitation when guanosine was mixed with silicotungstic acid. A clear solution was obtained first at about 100ºC, and it immediately re-precipitated in the pipette when taking out aliquots for the kinetic analysis which complicated the analysis. The rate constant for the deglycosylation of guanosine by phosphotungstate was estimated to 0.059 min^{-1} from the first-order plot (Supplementary Figure S9).

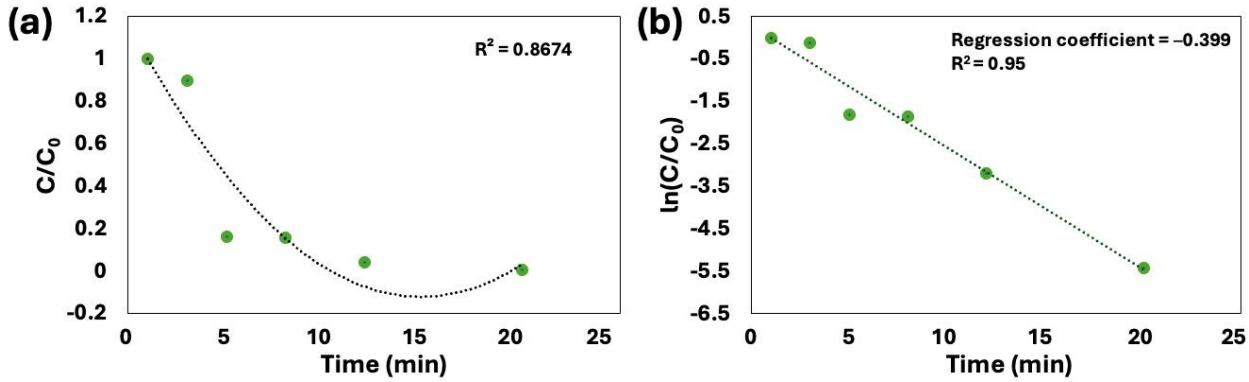

Figure 10. Kinetic plots of the deglycosylation of guanosine by silicotungstate, (a) C/C_0 plot and (b) first-order plot.

Combination of the obtained structural and kinetic data indicates that the actual mechanism in acidic deglycosylation of nucleosides is facilitated by specific interaction of POM with the C-N bond, where the POM negatively charged bridging oxygen atom acts as nucleophile facilitating charge separation and accumulation of the positive charge on the affected carbon atom. The latter is then attacked by water as replacing nucleophile forming a hydroxyl group on the sugar molecule and protonating the released amino base. The observed difference between silico- and phosphotungstate appears thus logical in the view of higher polarity in the POM core with less electronegative heteroelements atom inside. This explains also the inactivity of titania nanoparticles in the proposed catalysis path as in spite possessing even larger charge distribution in Ti-O bond, they are protonated under the investigated reaction conditions. Negatively charged

View Article Online
DOI: 10.1039/D6DT00402D

vanadium POMs have been observed to be contributing to inhibition of Ca^{2+}-ATPase via in the first hand charge interaction between the negatively charged POM and positively charged pockets of the enzyme.[33,34] Interaction we observed here differs principally from those between POMs and sugars, studies so far by NMR,[35] because the latter demonstrated only "normal" hydrogen bonds without any specific C…O(POM) interactions been detected. It is important to note that the most interesting in further studies would be to address POM reactivity towards nuclotides bearing phosphate linkages. Vanadium based POMs have in fact been observed to cleave phosphorylated organic species.[36] In this future work, we would expect also a pronounced activity of titania particles in the view of earlier demonstrated high affinity of TiO_2 surface to phosphate and phosphonate ligands.[37]

Diffusion ordered NMR spectroscopy (DOSY) was attempted on 1:1 mixtures of silicotungstic acid or phosphotungstic acid with guanosine to study their interaction in solution. However, as the solubility of the mixtures were so low, and as DOSY is much less sensitive than ^{1}H NMR; reliable DOSY spectrum could not be obtained. A comparison between the ^{1}H NMR spectrum of guanosine in 0.1 M HCl and guanosine with 1 eq. silicotungstic acid in. 0.1 M HCl is shown in supplementary Figure S8. The two samples contain the same amount of guanosine, but as silicotungstic acid is added, the intensity sharply decreases.

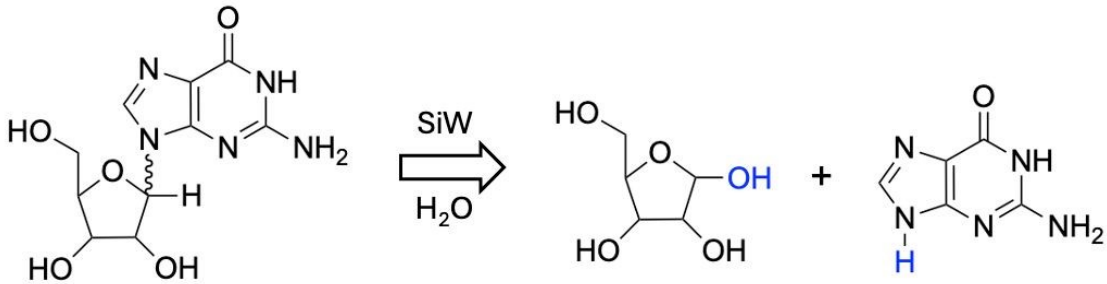

Scheme 3. Proposed degradation pathway of guanosine by silicotungstate.

Conclusions

In the current study we have investigated the potential deglycosylation of RNA by metal oxide nanoparticles, using the polyoxometalates phosphotungstic acid, silicotungstic acid and nano-TiO_2 (TiBALDH) as model systems for the metal oxides. We chose guanosine as a purine nucleoside (RNA base "G") and guanosine as a pyrimidine nucleoside (RNA base "C"). We crystallized a number of structural models illustrating the interaction between the nucleosides and the polyoxometalates. It was found that phosphotungstate and silicotungstate were able to cleave cytidine and guanosine by deglycosylation. However, no deglycosylation was seen for nano-TiO_2 under the investigated conditions.

Kinetic studies revealed guanosine to be more rapidly degraded than cytidine. With silicotungstic acid as catalyst guanosine was almost completely degraded to its guanine and

View Article Online
DOI: 10.1039/D6DT00402D

ribose components while cytidine remained virtually intact. This suggests a difference in reactivity between the purine and pyrimidine nucleobases. Based on structural information from the molecular models, we see π-metal interactions where the aromatic ring acts as acceptor of negative charge from the POM, forming charge-transfer complexes also supported by colored crystals. Both TiO_2 and the POM have negatively charge surfaces, though the POMs are much smaller than TiO_2.

Acknowledgements

The support from the Swedish Research Council (Vetenskapsrådet, project 2022-03971_VR), "Molecular mechanisms in oxide nanoparticle interactions with proteins", is gratefully acknowledged.

References

1. T. I. Shabatina, O. I. Vernaya, N. L. Shimanovskiy and M. Y. Melnikov, *Pharmaceutics*, 2023, **15**, 1181.
2. M. Aureliano, *BioChem*, 2025, **2**, 8–26.
3. G. Guedes, S. Wang, A. H. Santos and F. L. Sousa, *Eur. J. Inorg. Chem.*, 2020, **22**, 2121–2132.
4. A. Bijelic, M. Aureliano and A. Rompel, *Angew. Chem. Int. Ed.*, 2018, **58**, 2980–2999.
5. B. H. Greijer and V. G. Kessler, *CrysEngComm*, 2025, **27**, 1679.
6. D. E. S. Marcano, N. D. Savic, K. Declerck, S. A. M. Abdelhameed and T. N. Parac-Vogt, *Chem. Soc. Rev.*, 2024, **53**, 84–136.
7. A. Nefedova, F. G. Svensson, A. S. Vanetsev, P. Agback, T. Agback, S. Gohil, L. Kloo, T. Tätte, A. Ivask, G. A. Seisenbaeva and V. G. Kessler, *Inorg. Chem.*, 2024, **63**, 8556–8566.
8. K. Declerck, N. D. Savic, M. A. Moussawi, C. Seno, R. Pokratah, J. D. Roo and T. N. Parac-Vogt, *J. Am. Chem. Soc.*, 2024, **146**, 11400–11410.
9. M. A. Moussawi, F. de Azambuja and T. N. Parac-Vogt, *Angew. Chem. Int. Ed.*, 2025, **137**, e202423078.
10. S. S. Chacon, P. N. Reardon, C. J. Burgess, S. Purvine, R. K. Chu, T. R. Clauss, E. Walter, M. D.D., N. Washton and M. Kleber, *Environ. Sci. Technol.*, 2019, **53**, 3018–3026.
11. B. Greijer, A. Nefedova, T. Agback, P. Agback, V. Kisand, K. Rausalu, A. Vanetsev, G. A. Seisenbaeva, A. Ivask and V. G. Kessler, *Nanoscale*, 2025, **17**, 3728–3738.
12. S. Shigeta, S. Mori, T. Yamase, N. Yamamoto and N. Yamamoto, *Biomedicine & Pharmatherapy*, 2006, **60**, 211–219.
13. Y. F. Cao, J. Chen, Q. Bian, J. Ning, L. Yong, T. Ou, Y. Song and S. Wei, *Toxics*, 2023§, **11**, 882.

View Article Online
DOI: 10.1039/D6DT00402D

14. S. Shabbir, M. F. Kuylar, Z. A. Bhutta and P. A. Boruah, M., *BioNanoScience*, 2021, **11**, 621–632.
15. Z. Lou, Z. Li, Z. Xie, I. M. Sokolova, L. Song, W. J. G. M. Peijnenburg, M. Hu and Y. Wang, *Small*, 2020, **16**, 2002019.
16. J. Lojk, J. Repas, P. Veranic, V. B. Bregar and M. Pavlin, *Toxicol. Res.-Uk*, 2020, **432**, 152364.
17. B. Trouiller, A. Westbrook and P. S. Schiestl, *Cancer Research*, 2009, **69**, 8784–8789.
18. J. Petkovic, B. Zegura, M. Stevanovic, N. Drnovsek, D. Uskokovic, S. Novak and M. Filipic, *Nanotoxicol.*, 2010, **5**, 341–353.
19. M. Carriere, M. E. Arnal and T. Douki, *Mutation Res./Genetic Toxicol. Environ. Mutagenesis*, 2020, **854**, 503198.
20. K. Rajapakse, D. Drobne, D. Kastelec and R. Marinsek-Logar, *Nanotoxicol.*, 2012, **7**, 1043–1051.
21. M. Naya, N. Kobayashi, M. Ema, S. Kasamoto, M. Kukumoro, S. Takami, M. Nakajima, M. Hayashi and J. Nakanishi, *Regulatory Toxicol. Pharmacol.*, 2012, **62**, 1–6.
22. J. Petkovic, T. Kuzma, K. Rade, S. Novak and M. Filipic, *J. Hazardous Mater.*, 2011, **196**, 145–152.
23. E. J. Petersen, V. Reipa, S. S. Watson, D. H. Stanley, S. A. Rabb and B. C. Nelson, *Chem. Res. Toxicol.*, 2014, **27**, 1877–1884.
24. K. S. Gates, *Chem. Res. Toxicol.*,2009, **22**, 1747–1760.
25. R. B. Stockbridge, G. K. Schroder and R. Wolfenden, *Bioinorg. Chem.*, 2010, **38**, 224–228.
26. Y. Zhou, Z. Zhao, Q. Wu, J. Lei, H. Cui, J. Pan, R. Li and H. Lu, *Analyt. Chem.*, 2024, **96**, 17576–17585.
27. T. Prashar, F. De La Selle and K. A. Hudak, *RNA Biology*, 2023, **20**, 348–358.
28. A. L. Jacobs and P. Schär, *Chromosoma*, 2012, **121**, 1–20.
29. Y. Endo and K. Tsurugi, *J. Biol. Chem.*, 1988, **263**, 8735–8739.
30. G. A. Seisenbaeva, G. Daniel, J. M. Nedelec and V. G. Kessler, *Nanoscale*, 2013, **5**, 3330–3336.
31. F. G. Svensson, P. Simon and V. G. Kessler, *Inorg. Chim. Acta*, 2021, **526**, 120547.
32. M. Bischoff, N. Y. Kim, J. B. Joo and A. Marchioro, *J. Phys. Chem. Lett.*, 2022, **13**, 8677–8683.
33. B.R. Brito, H. de S. Camilo, A.F. da Cruz, R.R. Ribeiro, E.L. de Sá, C.C. de Oliveira, G. Fraquez, G. Klassen, M. Aureliano, G.G. Nunes, *Inorganics*, 2025, **13**, 306.
34. I. Meskini, F. Capet, G. Fraqueza, N. Dege, M.N. Tahir, B. Ayed, M. Aureliano, *Molecules*, 2025, **30**, 4334.
35. C.F.G.C. Geraldes, M.M.C.A. Castro, M.E. Saraiva, M. Aureliano, B.A. Dias, *J. Coord. Chem.*, 1988, **17**, 205-219.
36. M. Aureliano, J. Leta, V.M.C. Madeira, L. de Meis, B*iochem. Biophys. Res. Comm.*, 1994, 201, 155-159.

View Article Online
DOI: 10.1039/D6DT00402D

37. F.G. Svensson, G. Daniel, C.W. Tai, G.A. Seisenbaeva, V.G. Kessler, *RSC Advances*, 2020,**10**, 6873-6883.

Data availability statement for manuscript ART-02-2026-000402

View Article Online
DOI: 10.1039/D6DT00402D

All details of crystallographic data collection and refinement for the structures reported in this paper are available free of charge from the Cambridge Crystallographic data Centre, CCDC, following the link https://www.ccdc.cam.ac.uk citing deposition numbers **2530303-2530308.**

All other experimental details (preparation and characterization details, including FTIR, NMR, etc.) are available on request from the authors.